Invariant Set Based Vehicle Handling Improvement at Tire Saturation using Fuzzy Output Feedback

Na¨ıma Ait Oufroukh, Andr´e Benine-Neto, Zedjiga Yacine, Sa¨ıd Mammar, S´ebastien Glaser

***Abstract*— This paper firstly reviews of the analysis of the nonlinear behavior of the vehicle lateral dynamics. The $(\alpha_f, \dot{\alpha}_f)$ phase plane is used in order to quantify the stability region of the vehicle under different forward speed, steering angle and road adhesion. The tire-road interaction forces are modeled using Pacejka's magic formula. In a second step, the exact linear sectors procedure is used for representation of nonlinear functions in order to derive a Takagi-Sugeno (TS) fuzzy model. This model copes the behavior of the lateral tire forces including the linear, decreasing and saturated regions. Thereafter, a Takagi-Sugeno fuzzy output feedback is designed for yaw motion control. The controller acts through the steering of the front wheels and the differential braking torque generation. The computation of the controller is performed in such a way that the trajectories of the controlled vehicle remain inside an invariant set even when it is under disturbance input. This is achieved using quadratic boundedness theory and Lyapunov stability. Simulation tests show that the controlled car is able to satisfactorily perform standard maneuvers such as the ISO3888-2 transient maneuver and the roundabout maneuver.**

***Index Terms*— Vehicle handling, Fuzzy control, Output feedback, LMI, BMI.**

I. Introduction

Helping the driver maintain control of a vehicle in extreme lateral dynamics and even prevent that the vehicle reaches these situations is still an active research area. Electronic stability control systems (ESC) use independent wheel braking as an additional control input in order to conform the lateral dynamics, mainly the yaw rate value, to the driver intended set point which is sensed from the steering angle [4], [15]. In fact, bifurcation analysis has shown that the stability region is limited. The region could be quantified in the sideslip angle - yaw rate phase plane or in the sideslip angle rate and sideslip angle phase plane [14]. The extent of the stability region is function of the driver input on the steering wheel, the road adhesion and the longitudinal speed.

In parallel, vehicle handling has been also investigated through front and rear active steering [3], [6]. Using an additional steering angle of limited value solutions have been implemented in some series production [5]. However, action of steering will be really effective when x-by-wire systems will be spread in series vehicles. In fact, additional freedom factors in controller design architecture will be available [9].

Assuming the availability of such a technology, this paper proposes a dynamic fuzzy output feedback which uses both steering angle rate and differential braking. The dynamic output feedback formulation considered in this paper presents three main advantages: the use of only the yaw rate and the steering angle as measured variables, better flexibility to formulate the stabilization conditions and the ability to handle input or state constraints and bounded disturbances. This controller uses the property of quadratic boundedness and invariant set [2] which guarantees that each trajectory of the controlled vehicle that starts in the invariant set will not exceed it, hence the trajectories will be bounded inside it [8].

The paper is structured as follows: in Section 2 the vehicle model is presented, starting from the classical nonlinear bicycle model and some bifurcation properties associated with parameters variations and input values are reviewed. Thus, a Takagi-Sugeno fuzzy model is obtained, which allows an exact representation of the nonlinear behavior. In Section 3, the controller design is presented while simulation results are illustrated in Section 4. The conclusions wrap up the paper.

II. Vehicle Lateral Dynamics T-S Model

As lateral control is concerned, a simple nonlinear model of a vehicle is obtained by neglecting the roll and pitch motions. This model includes the lateral translational motion and the yaw motion (Fig. 1). The two wheels of each axle are lumped into one located at its center. This leads to the vehicle bicycle model. The lateral forces between each tire and the road surface are added at each axle leading to two resulting forces $f_f(\alpha_f) = f_{y1} + f_{y2}$ and $f_r(\alpha_r) = f_{y3} + f_{y4}$ at the front and rear wheels of the bicycle model respectively. These forces, which will be detailed below, are function of the front and rear tires sideslip angle, denoted α_f and α_r respectively.

The lateral translation and rotational yaw motion equations written in the vehicle fixed frame take the following form:

$$\begin{bmatrix} mv\left(\dot{\beta}+r\right) \\ J\dot{r} \end{bmatrix} = \begin{bmatrix} 1 & 1 & 0 \\ l_f & -l_r & 1 \end{bmatrix} \begin{bmatrix} f_f(\alpha_f) \\ f_r(\alpha_r) \\ T_z \end{bmatrix} \quad (1)$$

where β is the vehicle side slip angle, $\dot{\psi} = r$ is the yaw rate and T_z is the yaw moment input applied by differential wheel braking. m is the vehicle mass and J is the vehicle moment of inertia. The vehicle center of gravity is located

S. Mammar, N. Ait Oufroukh and Z. Yacine are with Université d'Évry Val d'Essonne, France. IBISC: Informatique, Biologie Intégrative et Systèmes Complexes - EA 4526, 40 rue du Pelvoux CE1455, 91020, Evry, Cedex, France, (e-mail: naima.aitoufroukh, said.mammar@iup.univ-evry.fr, yacine.zedjiga@live.fr).

A. Benine-Neto and S. Glaser are with IFSTTAR - LIVIC Laboratoire sur les Interactions Véhicule-Infrastructure-Conducteur. 14, route de la Minière, Bât 824, 78000, Versailles, France, e-mail: (sebastien.glaser, andre.benine-neto@ifsttar.fr).

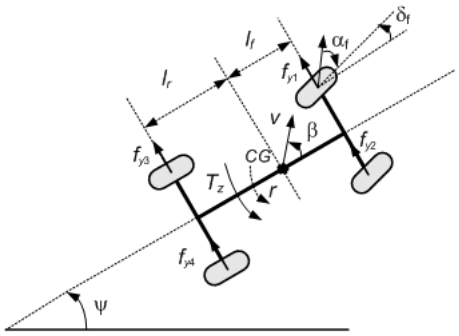

Fig. 1. Vehicle model.

at a distance l_f from the front axle and a distance l_r from the rear axle, as shown in Fig. 1. The vehicle parameters values are listed in Table I in the Appendix.

Assuming that the angles remain small, the front and the rear sideslip angles are given by:

$$\begin{aligned} \alpha_f &= \delta_f - \left(\beta + \tfrac{l_f}{v} r\right) \\ \alpha_r &= -\beta + \tfrac{l_r}{v} r \end{aligned} \tag{2}$$

A. Lateral tire forces model

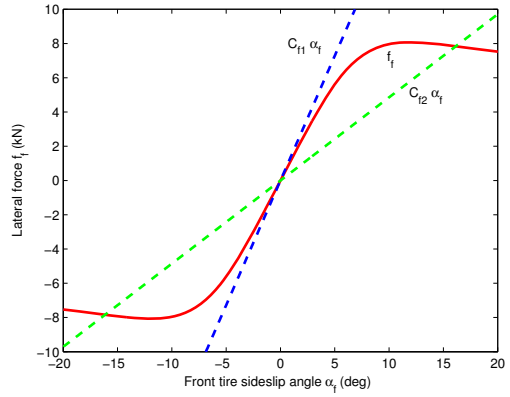

Fig. 2. Tire lateral force given by the pacejka model and sector based approximation.

Here, the well known Pacejka's formula [10] is used to represent the efforts exerted on each tire (Fig. 2). Lateral forces of front and rear tires are function of the side slip angle α_i at the tire-road contact location. The road adhesion μ, the normal force f_{ni} and the slip ratio which are considered constant. Here, the index j stands for f (front) or r (rear):

$$\begin{aligned} &f_j(\alpha_j) = \\ &d_j \sin\left(c_j \cdot \tan^{-1}(b_j(1-e_j)\alpha_j + e_j \cdot tan^{-1}(b_j\alpha_j))\right) \end{aligned} \tag{3}$$

The adhesion coefficient and the normal force acting on each tire are embedded inside the parameters b_j, c_j, d_j and e_j. See [6] for further details. The definition and the value of the above parameters are described in the appendix at the end of the paper.

The shape of the lateral force is as follows: A first linear domain for small sideslip angle allows to define a slope factor called the tire cornering stiffness coefficient. As the sideslip angle increases, the tire enters a nonlinear operating zone where the lateral force saturates.

B. Bifurcation analysis

The vehicle trajectories are simulated in different conditions in order to quantify the extent of stability region. The front tires sideslip angle and rate are chosen as the phase plane for the plot of the trajectories. Results shown in Fig. 3 are obtained for zero steering angle and maximum road adhesion ($\mu = 1$). The stability region is symmetric around the origin. When the steering angle is set to $0.02 rad/s$, the equilibrium points move towards a positive value, which leads to a decrease of the stability margin (Fig. 4). Returning to a zero steering angle while decreasing the road adhesion to ($\mu = 0.3$). The shrinkage of the original stability region is obvious in Fig. 5. Finally, when the steering angle is set again to 1.15 deg while maintaining the same road adhesion the stability region vanishes (Fig. 6).

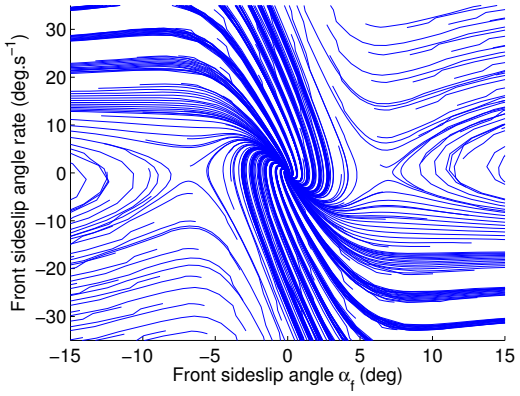

Fig. 3. $(\alpha_f, \dot{\alpha}_f)$, plane for $\delta_f = 0.0$ deg, $v = 30 m/s$ and $\mu = 1$.

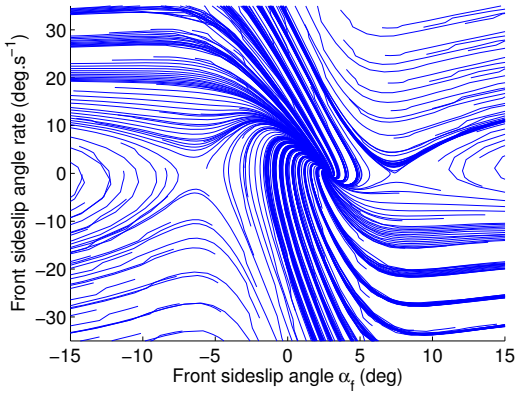

Fig. 4. $(\alpha_f, \dot{\alpha}_f)$, plane for $\delta_f = 1.15$ deg, $v = 30 m/s$ and $\mu = 1$.

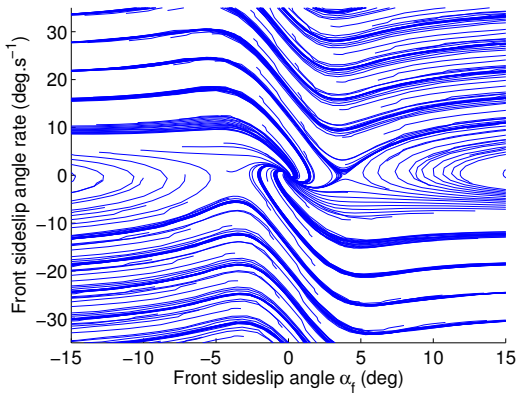

Fig. 5. $(\alpha_f, \dot{\alpha}_f)$, plane for $\delta_f = 0\,\text{deg}$, $v = 30m/s$ and $\mu = 0.3$.

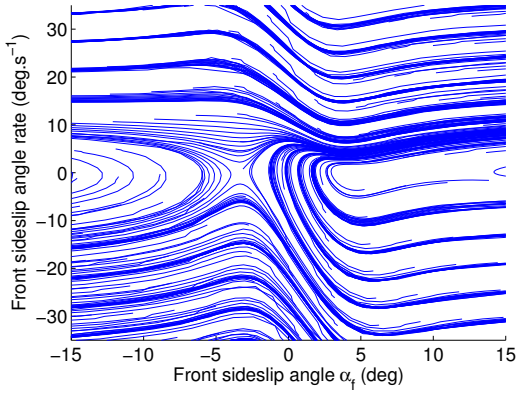

Fig. 6. $(\alpha_f, \dot{\alpha}_f)$, plane for $\delta_f = 1.15\,\text{deg}$, $v = 30m/s$ and $\mu = 0.3$.

The goal now is to achieve a Takagi-Sugeno fuzzy model which covers the entire operating domain (linear and non-linear) of the forces [12].

C. Four rules Takagi-Sugeno vehicle fuzzy model

The nonlinear vehicle model is transformed into a four rules Takagi-Sugeno (T-S) fuzzy model according to the values of the front and rear cornering stiffnesses:

- if $|\alpha_f|$ is m_1 and $|\alpha_r|$ is n_1 then $\begin{cases} f_f = c_{f_1}\alpha_f \\ f_r = c_{r_1}\alpha_r \end{cases}$
- if $|\alpha_f|$ is m_2 and $|\alpha_r|$ is n_1 then $\begin{cases} f_f = c_{f_2}\alpha_f \\ f_r = c_{r_1}\alpha_r \end{cases}$
- if $|\alpha_f|$ is m_1 and $|\alpha_r|$ is n_2 then $\begin{cases} f_f = c_{f_1}\alpha_f \\ f_r = c_{r_2}\alpha_r \end{cases}$
- if $|\alpha_f|$ is m_2 and $|\alpha_r|$ is n_2 then $\begin{cases} f_f = c_{f_2}\alpha_f \\ f_r = c_{r_2}\alpha_r \end{cases}$

The membership functions m_i and n_i $(i = 1,2)$ are determined by the approximation method of nonlinear function by linear sectors. Coefficients c_{f_i} and c_{r_i} $(i = 1,2)$ represent the tire cornering stiffnesses associated to each sector. In fact they also represent the slope of the limits of the sectors which include the tire forces (Fig. 2). For example, given two coefficients c_{f_1} and c_{f_2}, chosen according to the expected road adhesion and driving conditions, one can determine the membership functions $m_1(\alpha_f)$ and $m_2(\alpha_f)$. The evolution of the two functions m_1 and m_2 as functions of the sideslip angle are shown in Fig. 7. They are obtained with numerical values: $c_{f_1} = 1.2c_f$ and $c_{f_2} = 0.6c_f$. It is important to outline that this sector representation is an exact approximation of the nonlinear system.

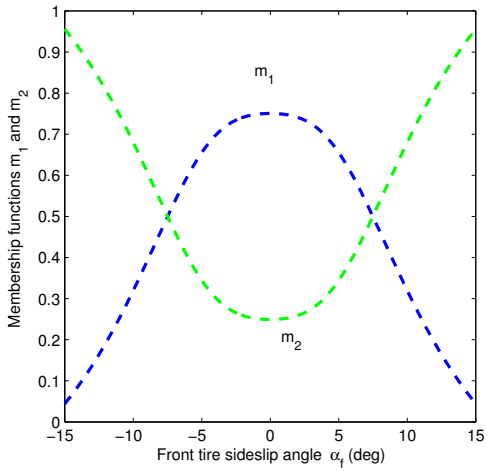

Fig. 7. Membership functions m_1 and m_2 associated to the front tire contact forces.

The membership functions n_1 and n_2 for the rear tire forces are obtained by the same procedure. Finally, one can write:

$$\begin{cases} f_f = \left[(h_1+h_3)c_{f_1} + (h_2+h_4)c_{f_2}\right]\alpha_f \\ f_r = \left[(h_1+h_2)c_{r_1} + (h_3+h_4)c_{r_2}\right]\alpha_r \end{cases} \tag{4}$$

with $h_1 = m_1 \times n_1$, $h_2 = m_2 \times n_1$, $h_3 = m_1 \times n_2$ and $h_4 = m_2 \times n_2$.

In order to have the front and the rear sideslip angle as state vector components, let us define the state $\bar{x} = [\alpha_f, \alpha_r, \delta_f]^T$ and the control input $u = [\dot{\delta}_f, T_z]^T$, the fuzzy system takes the form:

$$\dot{\bar{x}} = \sum_{i=1}^{4} h_i(\alpha_f, \alpha_r)\bar{A}_i\bar{x} + \bar{B}u \tag{5}$$

where

$$\bar{A}_i = \begin{bmatrix} a_{11i} & a_{12i} & a_{13} \\ a_{21i} & a_{22i} & a_{23} \\ 0 & 0 & 0 \end{bmatrix}, \bar{B} = \begin{bmatrix} 1 & -\frac{l_f}{Jv} \\ 0 & \frac{l_r}{Jv} \\ 1 & 0 \end{bmatrix} \tag{6}$$

where

$$\begin{cases} a_{11i} = -\frac{v}{l_f+l_r} - \frac{1}{v}\left(\frac{1}{m} + \frac{l_r l_f}{J}\right)c'_{fi}, \\ a_{12i} = \frac{v}{l_f+l_r} - \frac{1}{v}\left(\frac{1}{m} - \frac{l_f l_r}{J}\right)c'_{r_i}, \\ a_{21i} = -\frac{v}{l_f+l_r} - \frac{1}{v}\left(\frac{1}{m} - \frac{l_r^2}{J}\right)c'_{fi}, \\ a_{22i} = \frac{v}{l_f+l_r} - \frac{1}{v}\left(\frac{1}{m} + \frac{l_r^2}{J}\right)c'_{r_i}, \\ a_{13} = \frac{v}{l_f+l_r}, \\ a_{23} = \frac{v}{l_f+l_r}. \end{cases}$$

where $c'_{fi} = c_{f1}$ for $i = 1,3$ and $c'_{fi} = c_{f2}$ for $i = 2,4$. Similarly, $c'_{ri} = c_{r1}$ for $i = 1,2$ and $c'_{ri} = c_{r2}$ for $i = 3,4$.

D. Reference yaw rate tracking

Ideally, the vehicle should respond to driver's steering angle δ_d as a speed depended yaw rate reference steady state value with almost constant settling time. A desired transfer function between δ_d and r, is then sought. In order to ensure at nominal speed, the same steady state value for the controlled and the conventional car, the reference model is chosen as a first order transfer function with the same steady state gain as the conventional car. It is of the form $r_d = \frac{K_d(v)}{\tau s+1}\delta_d$. The speed dependent steady state gain is $K_d(v)$, derived from the nominal linear bicycle model, and $\tau = 0.2$ sec.

In order to ensure that the yaw rate reference value is achieved in steady state, the integral z of the yaw rate tracking error is added as state a variable:

$$\dot{z} = r - r_d = \frac{\delta_f + \alpha_r - \alpha_f}{l_f + l_r} v - r_d \tag{7}$$

This variable is thus added to the previous third order model (5) while the desired yaw rate is considered as a disturbance. The fuzzy model is finally discretized at a sample time of $T = 0.005$ sec. The final fuzzy model is of the form:

$$\begin{array}{l} x(t+1) = \sum_{i=1}^{4} h_i\left(\alpha_f, \alpha_r\right) A_i x(t) + Bu(t) + Ew(t) \\ y(t) = Cx(t) + Dw(t) \end{array} \tag{8}$$

where $x = [\alpha_f, \alpha_r, \delta_f, z]^T$ and $y(t) = [r, z]^T$. The disturbance $w(t) = r_d(t) \in \varepsilon_Q = \left\{w \in \mathscr{R} / w^T Q w \leq 1\right\}$ is bounded. Matrices A_i and B can be easily derived from equations (6) and (7). This discrete time fuzzy system is characterized by common B, E and C matrices. This property simplifies drastically the stability and performance conditions as only simple summations are involved.

III. Dynamic output feedback fuzzy controller

In the following, a dynamic output feedback fuzzy controller is sought. It has the form:

$$\begin{array}{l} x_c(t+1) = \sum_{i=1}^{4} h_i\left(\alpha_f, \alpha_r\right) A_c^i x_c(t) + B_c y(t) \\ u(t) = C_c x_c(t) + D_c y(t) \end{array} \tag{9}$$

where $x_c \in \mathscr{R}^4$ is the controller state; $\{A_c^i, B_c, C_c, D_c\}$ are matrices to be designed.

This controller uses the parallel distributed compensation (PDC) concept of the fuzzy system control. In this concept, each control rule is distributively designed for the corresponding rule of a T-S fuzzy model. Linear control theory can then be used to design controllers for each of the consequent part of the fuzzy system while ensuring the same properties for the fuzzy system.

As pointed out in [2], D_c is an important parameter for stabilization, and the controller structure is able to handle constraints on the input and the state. By combining (8) and (9), the augmented closed-loop fuzzy model is given by

$$\tilde{x}(t+1) = \sum_{i=1}^{4} h_i\left(\alpha_f, \alpha_r\right) \Phi_i \tilde{x}(t) + \Gamma w(t). \tag{10}$$

where $\tilde{x} = \begin{bmatrix} x \\ x_c \end{bmatrix}$, $\Phi_i = \begin{bmatrix} A_i + BD_cC & BC_c \\ B_cC & A_c^i \end{bmatrix}$ and $\Gamma = \begin{bmatrix} BD_cD + E \\ B_cD \end{bmatrix}$.

Let $\Phi_z = \sum_{i=1}^{4} h_i\left(\alpha_f, \alpha_r\right) \Phi_i$, the closed loop system takes the form: $\tilde{x}(t+1) = \Phi_z \tilde{x}(t) + \Gamma w(t)$.

A. Invariant set and output feedback PDC control

Assume that there exists a quadratic function $V(\tilde{x}) = \tilde{x}^T P \tilde{x}$, where P is a symmetric, positive definite matrix that satisfies, for all $\tilde{x}$, w satisfying (10), $w^T Q w \leq 1$, $V(\tilde{x}) \geq 1$, the condition [1]:

$$V(\tilde{x}(t+1)) \leq V(\tilde{x}(t)) \tag{11}$$

Consider the reachable set Λ defined by:

$$\begin{array}{rl} \Lambda \triangleq & \{\tilde{x}(T) | \tilde{x}, w \text{ satisfying (10)}, \\ & \tilde{x}(0) = 0, w^T Q w \leq 1, T \geq 0\} \end{array} \tag{12}$$

The set ε_P defined by:

$$\varepsilon_P = \{\tilde{x}(t) \in \mathscr{R}^8 | \tilde{x}(t)^T P \tilde{x}(t) \leq 1\}, \tag{13}$$

is an invariant set for the system (10) with $w \in \mathscr{R}$, $w^T Q w \leq 1$. This means that every trajectory that starts inside ε_P remains inside it for $t \to \infty$.

The existence of such a function $V(\tilde{x})$ means that the set ε_P is an outer approximation of the reachable set Λ.

ε_P is also an outer approximation of the reachable set

$$\begin{array}{rl} \Lambda^* \triangleq & \{\tilde{x}(T) | \tilde{x}, w \text{ satisfying equation (10)}, \\ & \tilde{x}(0) \in \varepsilon_P, w^T Q w \leq 1, T \geq 0\} \end{array} \tag{14}$$

B. Invariant set - quadratic boundedness

According to the previous considerations, the closed loop linear system $\tilde{x}(t+1) = \Phi_z \tilde{x}(t) + \Gamma w(t)$ is strictly quadratically bounded with a common Lyapunov matrix $P > 0$ for all allowable $w(t) \in \varepsilon_Q$, for $t > 0$, if $\tilde{x}(t)^T P \tilde{x}(t) > 1$ implies $\left(\Phi_z \tilde{x}(t) + \Gamma w(t)\right)^T P \left(\Phi_z \tilde{x}(t) + \Gamma w(t)\right) < \tilde{x}^T P \tilde{x}$, for any $w \in \varepsilon_Q$.

C. Constraints on state and control input

In addition, it is possible to handle constraints on the control signal and the state:

$$-\bar{u} \leq u(t) \leq \bar{u}, \quad -\bar{\Psi} \leq \Psi x(t+1) \leq \bar{\Psi}, \quad \forall t \geq 0 \tag{15}$$

where $\bar{u} = [\bar{u}_1, \bar{u}_2]^T$ with $\bar{u}_1 > 0$, $\bar{u}_2 > 0$ and $\bar{\Psi} := [\bar{\Psi}_1, \ldots, \bar{\Psi}_q]^T$ with $\bar{\Psi}_j > 0$, $j = 1, \ldots, q$, $\Psi \in \mathscr{R}^{q \times 4}$ and q is the number of imposed constraints. Notice that the bounds are provided separately on each state variables or a combination of state variables.

D. Controller synthesis

The controller is derived form BMI (Bilinear Matrix Inequalities) conditions obtained using the $S-$procedure and invoking the Schur complement. Further details are provided in [2] and [7]. The closed loop system without the disturbance is ensured to be asymptotically stable and at the same time, the reachable set for initial state values inside the invariant set is contained in this invariant set.

Under the proposed modeling approach, the desired yaw rate could be seen as an input disturbance under which the closed-loop system should remain stable with bounded values for the state vector components. More generally, the state variables should not exceed the bounds of a "safety zone", namely $|\alpha_f| \leq \alpha_f^M$, $|\alpha_r| \leq \alpha_r^M$ and $|\delta_f| \leq \delta_f^M$. Thus, the state vector x has to be confined to a hypercube $L(Z^M)$ defined by the above bounds. Finally, the control input, the steering angle rate and the yaw moment, have to be bounded $\left|\dot{\delta}_f\right| \leq \dot{\delta}_f^M$ and $|T_z| \leq T_z^M$.

According to the equation (15), control limitation is given by $\bar{u} = [\dot{\delta}_f^M, T_z^M]$, while state limitation is given by $\bar{\Psi} = [\alpha_f^M, \alpha_r^M, \delta_f^M]^T$ and $\Psi = \begin{bmatrix} I_3 & 0 \end{bmatrix}$.

The PDC output feedback controller was synthesized with the following numerical values:

$$\delta_f^M = 6\,\text{deg}, \quad \dot{\delta}_f^M = 100\,\text{deg}/s,$$
$$T_z^M = 10KN \quad \alpha_f^M = \alpha_r^M = 13\,\text{deg},$$

The selected values ensure that the uncontrolled vehicle saddle points are inside the invariant set. These design parameters could be adjusted to handle the trade-off between safety constraints and comfort specifications.

The achieved Q is 5, which ensures that the constraints are verified for a disturbance of a magnitude less than $0.447 rad/s$ at the considered longitudinal speed of $20 m/s$. In fact, the maximum value is constrained by [11]:

$$r_{d_{\max}} = 0.85 \frac{g}{v} \tag{16}$$

IV. Simulation tests

In order to prove the assistance ability to maintain the dynamic vehicle stability in extreme conditions, several types of maneuvers have been defined to test the ESC systems. Among them, double lane-change manoeuvre defined in ISO 3888-2 standard and the roundabout maneuver are tested.

A. Testing for the roundabout maneuver

The vehicle speed is set $80 km/h$ while the steering angle at the front tires is chosen at $3 deg$. Fig. 8 shows that the controlled vehicle trajectory is very close to that of the reference vehicle. The uncontrolled vehicle experiences a higher offset. This simulation demonstrated the ability of the proposed controller to make the controlled vehicle follow a reference yaw rate.

B. Testing for the ISO 3888-2 maneuver

The ISO 3888-2 double lane-change maneuver setup is depicted in Fig. 9-a. The maneuver is carried out with and without the controller at the same speed of $80 km/h$. During the maneuver, the throttle is released. The driver initiates the maneuver by applying the steering angle shown in dashed line in Fig. 9-b. The dashed plot of Fig. 9-a highlights that the uncontrolled vehicle fails to perform the maneuver, as it exits the track, the controlled vehicle is able to perform it (solid line). In this situation the driver applied steering angle is too high (dashed line in Fig. 9-b) while the steering angle of the controlled vehicle is limited to the admissible

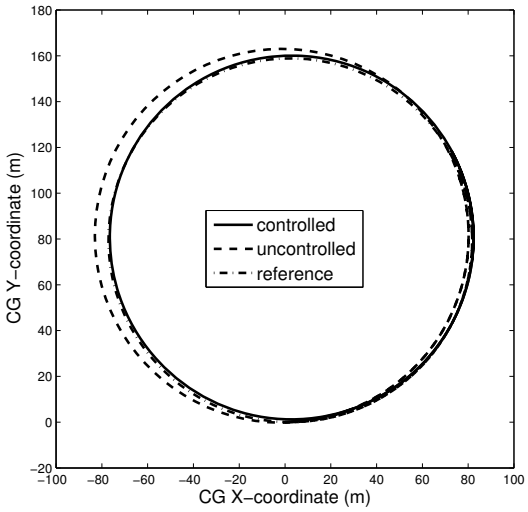

Fig. 8. Vehicle trajectory for the roundabout maneuver. Dashed line for the uncontrolled vehicle and solid line for the controlled one. Reference vehicle in dash-dot line

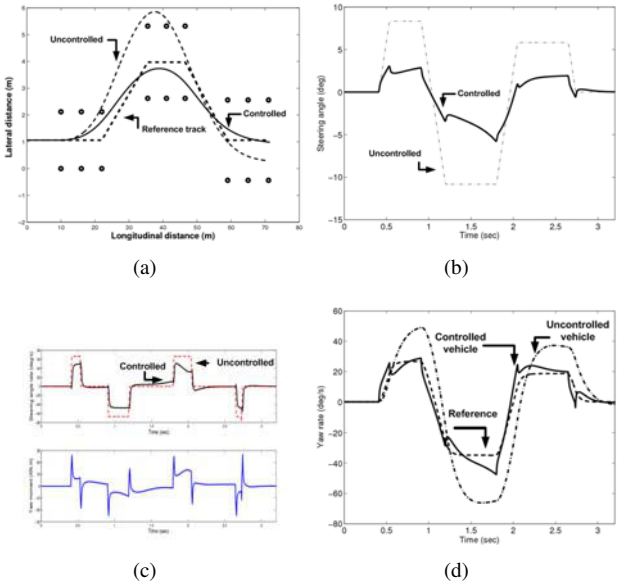

(a) (b) (c) (d)

Fig. 9. ISO3888-2 maneuver: Trajectory, steering angle, steering angle rate, yaw moment and Yaw rate for the uncontrolled and the controlled vehicles.

safety value, as shown by the solid line in Fig. 9-b. The steering angle rate is depicted in the top plot of Fig. 9-c and is limited for the controlled car. Fig. 9-c shows also that the controller shares the effort on the steering angle rate and the yaw moment, respectively. Fig. 9-d shows that the controlled car yaw rate is closer to the reference one than the yaw rate of the uncontrolled vehicle (dashed line). The contribution of each sub-controller according to the actual vehicle dynamics is shown in Fig. 10. Finally, Fig. 11-a and 11-b provide the developed sideslip angles at the front and rear tires. The corresponding front and rear forces are shown in Fig. 11-c and 11-d.

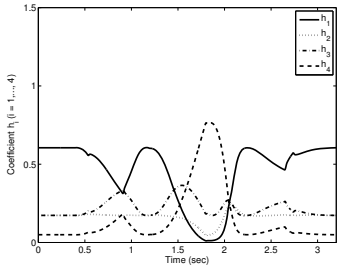

Fig. 10. ISO3888-2 maneuver: Coefficients h_i reflecting the contribution of each sub-controller for the controlled vehicles.

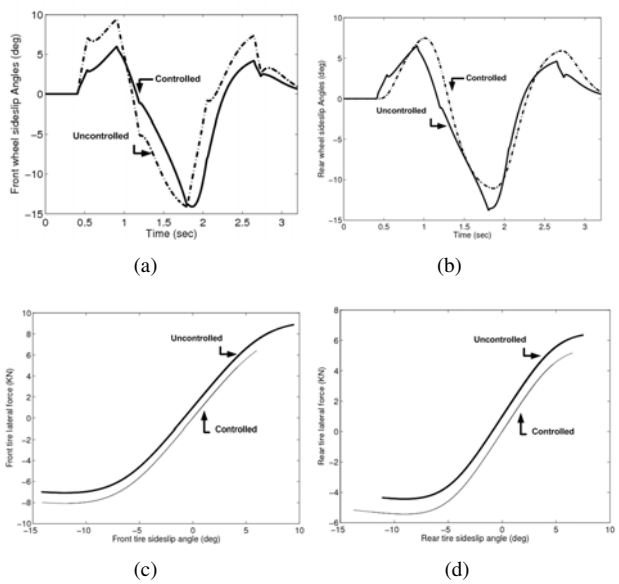

(a) (b)

(c) (d)

Fig. 11. ISO3888-2 maneuver: Front and rear tire sideslip angle and corresponding lateral forces for the uncontrolled (dash-dot) and the controlled vehicles (solid), with vertical offset for the uncontrolled one for better display.

It is clear that the saturation zones are reached by the uncontrolled and the controlled vehicles. However, the incursions into the saturation zones are more limited and vehicle control is ensured there.

V. Conclusion

In this paper the nonlinear behavior of the vehicle lateral dynamics has been highlighted. The stability regions are simply depicted in the $(\alpha_f, \dot{\alpha}_f)$ phase plane. The design and the test of an integrated steering and differential braking control for yaw moment generation have been described. Controlled vehicle trajectories are confined inside an invariant set under bounded disturbance input. An output feedback fuzzy controller constituted by four sub-controllers handles constraints on the state variables and the control inputs. Simulation tests have shown that the controlled vehicle is able to achieve the roundabout and the ISO 3888-2 transient maneuvers where the uncontrolled vehicle fails. Future works will address controller activation strategies according vehicle state location in the $(\alpha_f, \dot{\alpha}_f)$ plane.

Appendix

TABLE I

Vehicle parameters.

m	Vehicle total mass 1600 kg.
c_f	Front cornering stiffness 40000 N/rad.
c_r	Rear cornering stiffness 35000 N/rad.
J	Vehicle yaw moment of inertia 2454 kg$\cdot m^2$.
l_f	Distance form CG to front axle 1.22m.
l_r	Distance from CG to rear axle 1.44m.
v	Longitudinal velocity.

TABLE II

Tire model parameters.

Tire	b_i	c_i	d_i	e_i
Front $(j = f)$	8.3278	1.1009	4536.0	-1.661
Rear $(j = r)$	11.6590	1.1009	3671.6	-1.542

Acknowlegment

This work has been partially financed by the French FUI project E-MOTIVE.

References

[1] A. Alessandri, M. Baglietto, G. Battistelli, Design of state estimators for uncertain linear systems using quadratic boundedness. Automatica, 42, 497-502, 2006.

[2] B. Ding, Quadratic boundedness via dynamic output feedback for constrained nonlinear systems in Takagi–Sugeno's form, Automatica, vol. 45, N° 9, pp. 2093-2098, 2009.

[3] J. C. Gerdes et E. J. Rossetter A Unified Approach to Driver Assistance Systems Based on Artificial Potential Fields Authors. Journal of Dynamic Systems, Measurement and Control, Vol. 123, No. 3, pp. 431-438, 2001.

[4] M.J. Hancock, R.A. Williams, T.J. Gordon, M.C. Best, A comparison of braking and differential control of road vehicle yaw-sideslip dynamics, Proceedings of IMechE., Part D: Automobile Engineering, V.219, pp. 309-327, 2005.

[5] P. Kohen and M. Ecrick, Active Steering - The BMW Approach Towards Modern Steering Technology, SAE Technical Paper No. 2004-01-1105, 2004.

[6] S. Mammar and D. Koenig, Vehicle Handling improvement by Active Steering, Vehicle Sys. Dyn. Journal, vol 38, No3, pp. 211-242, 2002.

[7] S. Mammar, A. Benine Neto, S. Glaser, N. Aït Oufroukh, Vehicle Handling Improvement by Fuzzy Explicit Nonlinear Tire Forces Parametrization, Chinise Control and Decision Conference, 2011.

[8] N. Minoiu, M. Netto, S. Mammar, B. Lusetti, Driver steering assistance for lane departure avoidance, Control Engineering Practice, Vol. 17, No 6, pp. 642-651, 2009.

[9] E. Ono, Y. Hattori, Y. Muragishi, K. Koibushi, Vehicle Dynamics Integrated Control for Four-Wheel-Distributed Steering and Four-Wheel-Distributed Traction/Braking Systems, Vehicle System Dynamics, V.44, No.2, pp. 139-151, 2006.

[10] H. B. Pacejka, *Tyre and Vehicle Dynamics*, p 511- 562 , Delft University of Technology, 2002.

[11] Rajamani R., Vehicle Dynamics and Control, Springer, New-York, 2006.

[12] T. Takagi, M. Sugeno, Fuzzy identification of systems and its application to modeling and control, IEEE Trans. Systems Man Cybern. 15, pp. 116-132, 1985.

[13] J. Tjoennas and T. A. Johansen, Adaptive Optimizing Dynamic Control Allocation Algorithm for Yaw Stabilization of an Automotive Vehicle using Brakes, in Control and Automation, 2006. MED '06. 14th Mediterranean Conference on, 2006, pp. 1-6.

[14] H.D. Tuan, E. Ono, S. Hosoe, S. Doi, Bifurcation in Vehicle Dynamics and Robust Front Wheel Steering Control. IEEE Transactions on Control Systems Technology, 6, pp. 412-421, 1998.

[15] A.T.V. Zanten, Bosch ESP Systems: 5 Years of Experience, SAE Technical Paper No. 2000-01-1633, 2000.